A solid-state hybrid density functional theory study of Prussian blue analogues and related chlorides at pressure

2008 J. Phys.: Condens. Matter 20 335231

(http://iopscience.iop.org/0953-8984/20/33/335231)

J. Phys.: Condens. Matter **20** (2008) 335231 (13pp) doi:10.1088/0953-8984/20/33/335231

A solid-state hybrid density functional theory study of Prussian blue analogues and related chlorides at pressure

Derek S Middlemiss, Lorreta M Lawton and Chick C Wilson

Department of Chemistry and WestCHEM Research School,
University Avenue, University of Glasgow, Glasgow G12 8QQ, UK

E-mail: c.c.wilson@chem.gla.ac.uk

Received 14 May 2008, in final form 15 June 2008
Published 31 July 2008
Online at stacks.iop.org/JPhysCM/20/335231

Abstract

The variations with pressure in the structural, electronic and magnetic properties of a series of Prussian blue analogues (PBAs) $K^{I}M^{II}[Cr^{III}(CN)_6]$ ($M = V^{II}$, Mn^{II} and Ni^{II}) and associated isomorphous chlorides $K^{I}M^{II}Cr^{III}Cl_6$ are investigated within a series of solid-state hybrid density functional calculations. The sensitivity of the computed properties to the choice of Hamiltonian is tested by application of functionals containing 35%, 65% and 100% admixtures of Fock exchange. Magnetic coupling constants (J) are obtained at a range of cell volumes (V), with fits of the Bloch relationship ($J \propto V^{-\varepsilon}$, ε typically 3–4) yielding exponents ε in the ranges 5.16–6.34, 8.48–12.07 and 4.00–4.51 for the antiferromagnetic (AF) $V^{II}Cr^{III}$-, ferrimagnetic (FI) $Mn^{II}Cr^{III}$- and ferromagnetic (FO) $Ni^{II}Cr^{III}$ PBAs, respectively; and 3.33–4.99, 1.86–3.09 and 1.65–3.28 for the AF $V^{II}Cr^{III}$-, FO $Mn^{II}Cr^{III}$- and FO $Ni^{II}Cr^{III}$ chlorides, respectively. The $Mn^{II}Cr^{III}$ PBA range encloses the high values $\varepsilon \sim 9$–10 obtained in a recent joint experimental and theoretical study, and it is suggested that this strong magnetostructural effect arises due to the presence of competing AF and FO interactions in this material. Estimates of the spin ordering temperatures derived from the combination of the 35%-functional couplings with a mean field approach are in good agreement with experiment in the $V^{II}Cr^{III}$ and $Ni^{II}Cr^{III}$ PBAs, but are too low in the $Mn^{II}Cr^{III}$ system. The variations with pressure in the structural parameters, charges and spin moments are also detailed, the PBA and chloride energy–volume data yielding bulk moduli in the ranges 39–53 and 36–50 GPa, respectively. Finally, the energies governing CN^{-} ligand isomerization are estimated and successfully interpreted in terms of a simple crystal field stabilization model.

1. Introduction

The low densities and high molecular weights of the Prussian blue analogues (PBAs, figure 1) render them unsuitable for use as permanent magnets, but they do display a diverse range of properties of potential application in near future technologies, including high critical temperatures [1], pressure-induced pole inversions [2], optical transparency and photomagnetism [3]. Their high degree of structural flexibility and tolerance for variations in metal oxidation state have recently been exploited in the fabrication of magnetic nanoclusters and nanowires [4]. The magnetic properties of the PBAs under ambient conditions are now relatively well understood [5]. In particular, the dependence of the sign and strength of the coupling upon the combination of transition metal (TM) d-, and cyanide π- and π^{*}-orbital symmetries may be straightforwardly rationalized. Design strategies heeding these considerations have led to the syntheses of PBAs that retain spin order to temperatures as high as 376 K [1, 6, 7]. By way of contrast, however, the magnetic properties of these materials under non-equilibrium conditions remain relatively unexplored [8, 9]. The scarcity of such studies is symptomatic of the general difficulties encountered in detecting the magnetic response from samples enclosed within pressure cells. However, the recent development of large bore cells with low backgrounds has made sensitive magnetometry experiments under pressure possible [10]. The

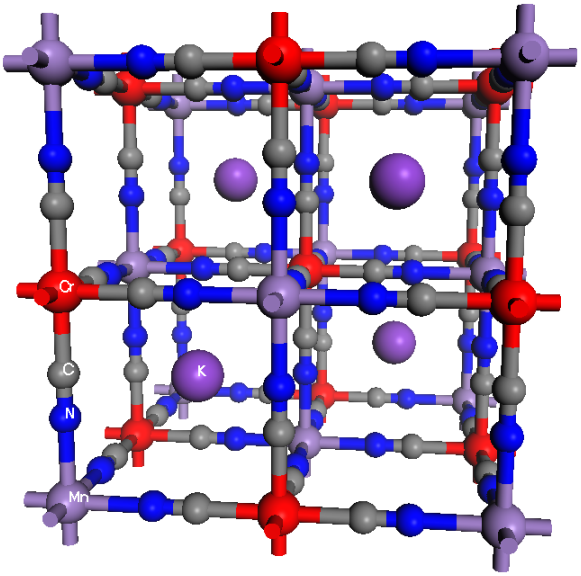

Figure 1. The conventional crystallographic cell of $K^{I}Mn^{II}[Cr^{III}(CN)_6]$.
(This figure is in colour only in the electronic version)

magnetostructural correlations of a material may then be accessed directly within a series of concurrent magnetometric and diffraction measurements over a range of pressures.

The model most commonly applied for the volume (V) or intersite distance (d) dependence of the magnetic interaction strength (J) in transition metal compounds is the phenomenological relationship

$$J \propto V^{-\varepsilon} = d^{-3\varepsilon}, \tag{1}$$

proposed by Bloch on the basis of studies of superexchange couplings in isomorphic oxides and fluorides [11–15]. The coupling constant J is usually defined in terms of a model magnetic Hamiltonian of the general form

$$\hat{H}_{\text{Spin}} = \tfrac{1}{2} J \sum_{ij}^{\text{nn}} S_i S_j, \tag{2}$$

where the index j spans the spins (S) nearest-neighbour (nn) to each site i. The exponent ε may be thought of as a magnetic Grüneisen constant, taking a material-dependent value that is typically in the range from 3 to 4 [11–15]. However, a recent combined experimental and theoretical study of a hydrated $Mn^{II}Cr^{III}$ PBA obtained much larger ε values in the range 9.03–9.97 [16], indicative of unusually strong magnetostructural correlations. The current work sets out to investigate through computations whether such large exponents are a property of PBAs in general, and whether they manifest in mixed—TM compounds bearing ligands other than cyanide. In addition to the ferrimagnetic (FI) $KMn^{II}[Cr^{III}(CN)_6]$ system considered previously [16], we extend our focus to include the strongly antiferromagnetic (AF) $KV^{II}[Cr^{III}(CN)_6]$, and ferromagnetic (FO) $KNi^{II}[Cr^{III}(CN)_6]$ compounds, and to structurally similar materials bearing Cl^- rather than CN^- ligands. It is likely that the chlorides will not be thermodynamically stable in the structure proposed, but our present interest in such lattices is limited to the insights they afford into the magnetism of the corresponding PBAs.

An analysis of the interactions arising between the singly-occupied TM d-orbitals in each compound makes for a useful preliminary. We anticipate that the nine pairwise $t_{2g}{}^3$–$t_{2g}{}^3$ interactions in the $V^{II}Cr^{III}$ systems will be AF in sign, with relative coupling strengths determined to a first approximation by high t_{2g}–$CN(\pi)$ and low t_{2g}–$Cl(\sigma)$ overlaps. The ordering temperature of the cyanide is consequently expected to be higher than that of the chloride. We anticipate that the nine t_{2g}^3–t_{2g}^3 interactions in the $Mn^{II}Cr^{III}$ systems will behave in a similar fashion, but we must also in this case consider the six FO e_g^2–t_{2g}^3 interactions possessing relative coupling strengths determined by low e_g–$CN(\pi)$ and high e_g–$Cl(\sigma)$ overlaps. Thus, we predict that the ground states of the cyanide and chloride will be FI and FO in nature respectively, and also that a complex magnetic response may emerge under compression, due to the fact that the AF and FO interaction components are likely to scale at different rates with intersite distance. Finally, the six FO e_g^2–t_{2g}^3 interactions in the $Ni^{II}Cr^{III}$ systems are expected to be similar to those in $Mn^{II}Cr^{III}$, leading us to anticipate a higher FO ordering temperature in the chloride than in the cyanide. It is hoped that the analysis of the magnetic response to pressure in the purely AF $V^{II}Cr^{III}$ and FO $Ni^{II}Cr^{III}$ PBAs will be of assistance in rationalizing the large ε value obtained in our previous study of $KMn^{II}[Cr^{III}(CN)_6]$ [16].

The literature relating to the PBAs includes a substantial body of theoretical work. Harrison *et al* have applied the UHF and B3LYP methods to solid-state models of $V^{II}Cr^{III}$, $Mn^{II}Cr^{III}$ and $Ni^{II}Cr^{III}$ PBAs [17, 18], finding magnetic ground states in agreement with experiment, and magnetic energy differences correlating with the known critical temperatures. Ruiz *et al* have performed cluster calculations as part of a systematic search for PBAs with higher ordering temperatures than the well-known $V^{II}Cr^{III}$ system [19], while other workers have studied magnetism and CN linkage isomerism in bi-, and crystal field excitations in mono-metallic clusters [20, 21]. Finally, Weihe and Güdel provide an analysis of magnetic coupling through the cyanide bridge in terms of a valence bond configuration interaction model, arriving at a simple two-parameter model that reproduces known J values well [22]. More generally, the current calculations are guided by and contribute toward a large number of theoretical determinations of coupling constants in TM compounds from solid-state broken symmetry calculations [23–28].

We seek to derive reliable theoretical values for the magnetic Grüneisen constants, ε, of the six anhydrous cyanides and chlorides, and to provide some estimate of their spin ordering temperatures. Previous studies have demonstrated the utility and accuracy of hybrid density functionals for the same properties within a wide range of TM compounds [23–28]. We shall also comment upon the electronic structure of these materials, focusing in particular upon the character of the valence and conduction band edges. Finally, we shall estimate the energies governing CN^- ligand isomerism, and detail the effects of isomerization upon magnetic coupling strengths and local lattice geometries.

2. Computational methods

The total energies and electronic structure of the FO and FI (or AF) magnetic states of each material were obtained from solid-state calculations using the CRYSTAL03 localized basis set code [29]. Standard Pople 6–311G* (or 1s[6], 2sp[3], 3sp[1], 4sp[1], 3d[1] in the *shell[number of primitive functions]* nomenclature) basis sets were initially adopted for C and N atoms; the exponents and contraction coefficients of the 2sp-, 3sp-, 4sp- and 3d-shells were then re-optimized iteratively within UHF calculations upon FO $KMn[Cr(CN)_6]$. An 8–6311G (1s[8], 2sp[6], 3sp[3], 4sp[1], 5sp[1]) basis set optimized for the isolated anion was adopted for Cl^-, and the 4sp- and 5sp-shell exponents re-optimized iteratively within UHF calculations upon FO $KMnCrCl_6$. Metal ions were represented by standard 8–6411d41G (1s[8], 2sp[6], 3sp[4], 4sp[1], 5sp[1], 3d[4], 4d[1]) basis sets optimized previously for the Cr^{III}, V^{II}, Mn^{II}, and Ni^{II} charge states, along with a standard 8–6511G (1s[8], 2sp[6], 3sp[5], 4sp[1], 5sp[1]) basis optimized previously for K^I. Further discussion of the application of Gaussian basis sets to solid-state calculations is available within the texts by Dovesi *et al* [30] and Pisani *et al* [31], and in the recent monograph by Martin [32]. An isotropic Monkhorst–Pack reciprocal space sampling mesh with a shrinking factor of 8, and Coulomb and exchange series truncation thresholds of 10^{-7}, 10^{-7}, 10^{-7}, 10^{-7} and 10^{-14} provided well converged coupling constants, where the parameters are as defined in the CRYSTAL03 documentation [29]. The ranges in each of our calculated properties were established by application of three hybrid Hamiltonians of the form

$$f^{\mathrm{xc}} = \frac{100 - F_0}{100}\left(f^{\mathrm{x}}_{\mathrm{LSDA}} + 0.9\Delta f^{\mathrm{x}}_{\mathrm{B88}}\right) + \frac{F_0}{100} f^{\mathrm{x}}_{\mathrm{UHF}} + 0.81 f^{\mathrm{c}}_{\mathrm{LYP}} + 0.19 f^{\mathrm{c}}_{\mathrm{VWN}}, \quad (3)$$

in which x and c denote exchange and correlation contributions; LSDA, B88 and UHF, the local spin density, Becke–88 [33] and spin-unrestricted Hartree–Fock exchange potentials respectively; and VWN and LYP, the Vosko, Wilk and Nusair [34] and Lee, Yang and Parr [35] correlation functionals respectively. The F_0 parameter controls the admixture of Fock exchange in the Hamiltonian, and may essentially be chosen arbitrarily. Setting $F_0 = 20\%$ yields the well-known B3LYP functional [36], but in the current work, we employed values of 35%, 65% and 100%, along with the uncorrelated UHF Hamiltonian ($f^{\mathrm{xc}} = f^{\mathrm{x}}_{\mathrm{UHF}}$). The $F_0 = 35\%$ Hamiltonian was included on the basis that it has previously been shown to give magnetic coupling constants in good agreement with experimental values in a wide range of TM bearing compounds [25]. The hybrid functional calculations used the UHF charge- and spin densities for initialization and proceeded to convergence without constraint. The total energies of FI (or AF) and FO states were obtained for lattice constants within a range from approximately +5 to −10% of the optimized values, yielding pressures $P = -\frac{\partial E}{\partial V}$ in the magnetic ground states ranging from approximately −5 to +15 GPa. The internal structural degrees of freedom at each cell volume were optimized by application of a modified Berny algorithm with an energy tolerance of $10^{-7} E_{\mathrm{h}}$ and an RMS force tolerance of 0.0003 au. The Mulliken method was used to partition the charge and spin densities into atomic contributions. The absolute values provided by these analyses must be interpreted with caution, for they bear little formal meaning, are undoubtedly obtained with greater precision than any putatively 'real' measure of charge, and are known to display strong basis set dependence [37]. However, the relative variations in these quantities with change of pressure and Hamiltonian within a given compound are expected to be reliable. Further to this point, and with the aim of circumventing basis set dependence, we derive the atomic dynamical charges as one-third of the trace of the associated Born effective charge tensors [38]

$$Z_{ij} = V \left.\frac{\partial P_i}{\partial u_j}\right|_{\vec{E}=\vec{0}}, \quad (4)$$

where indices i and j run over Cartesian axes; and in which V denotes the cell volume, P the cell polarization vector, u the atomic displacement, and E the applied electric field; all as embodied within normal mode calculations [39, 40] incorporating Wannier–Boys localization [41]. The calculations are intensive, and so only a limited set of values for the PBAs at $F_0 = 35\%$ have been computed.

3. Results and discussion

3.1. Structural and equation-of-state parameters

Tables 1 (cyanides) and 2 (chlorides) present the optimized lattice constants (a) and bulk moduli

$$K_0 = V_0 \left.\frac{\partial^2 E}{\partial V^2}\right|_{V_0}, \quad (5)$$

obtained from fits of quartic functions to the respective energy–volume data, along with individual bond lengths (d) and their pressure derivatives (d') at equilibrium. We see that change of functional yields no clear trend in the cyanide and chloride lattice constants, whereas previous studies of the rocksalt-structured TM monoxides (TMOs) generally obtained values of a that fell as F_0 was increased [26, 27, 42]. The removal of LYP correlation with progress from the $F_0 = 100\%$ to UHF Hamiltonians leads to 2–3% increases in a over the $F_0 = 100\%$ value. We note also that the chloride lattice constants are all approximately 1 Å smaller than those of the corresponding cyanide. The variations in the cyanide and chloride lattice constants across the range of M^{II} cations closely parallel the ionic radii of the six-fold coordinated species [43], which fall in the order $r(Ni^{II}) < r(V^{II}) < r(Mn^{II})$. We find also that the M^{II}–N and M^{II}–Cl distances are all larger than the corresponding Cr^{III}–C and Cr^{III}–Cl distances, in keeping with the smaller Cr^{III} radius.

The bulk moduli increase progressively across the range from $F_0 = 35\%$ to 100% before decreasing sharply at the UHF level, in agreement with previous observations in the TMOs [26, 27, 42]. The values in the PBAs range from approximately 39 to 53 GPa, exceeding the experimental modulus of 27 GPa obtained within the earlier study of

Table 1. The variation with Fock exchange content (F_0) in the optimized lattice constants, a_0 (Å), bulk modulus at equilibrium, K_0 (GPa), metal-to-ligand bond lengths, d (Å) and pressure derivatives, d' (10^{-3} Å GPa^{-1}) for the equilibrium $V^{II}Cr^{III}$, $Mn^{II}Cr^{III}$ and $Ni^{II}Cr^{III}$ cyanide lattices in their ground AF, FI and FO states respectively.

F_0	a_0	K_0	d_{M-N}	d'_{M-N}	d_{C-N}	d'_{C-N}	d_{C-Cr}	d'_{C-Cr}
$V^{II}Cr^{III}$ (AF ground state)								
35	10.733	43.60	2.135	−21.1	1.151	−1.0	2.081	−15.1
65	10.791	45.10	2.164	−21.0	1.138	−1.0	2.094	−13.5
100	10.808	47.28	2.175	−20.4	1.125	−1.0	2.104	−13.8
UHF	11.068	39.63	2.244	−23.8	1.136	−1.1	2.154	−15.3
$Mn^{II}Cr^{III}$ (FI ground state)								
35	10.943	42.26	2.237	−22.3	1.150	−1.2	2.084	−15.0
65	10.946	44.18	2.239	−21.1	1.137	−1.2	2.097	−14.3
100	10.930	46.29	2.235	−20.5	1.125	−1.1	2.105	−13.5
UHF	11.185	39.34	2.301	−23.3	1.135	−1.2	2.157	−12.9
$Ni^{II}Cr^{III}$ (FO ground state)								
35	10.647	46.34	2.090	−16.0	1.149	−1.0	2.085	−12.9
65	10.661	50.66	2.098	−17.0	1.136	−1.1	2.096	−13.2
100	10.655	52.82	2.099	−16.5	1.124	−1.0	2.105	−12.5
UHF	10.908	44.14	2.164	−19.4	1.135	−1.2	2.155	−14.3

Table 2. The variation with Fock exchange content (F_0) in the optimized lattice constants, a_0 (Å), bulk modulus at equilibrium, K_0 (GPa), metal-to-ligand bond lengths, d (Å) and pressure derivatives, d' (10^{-3} Å GPa^{-1}) for the equilibrium $V^{II}Cr^{III}$, $Mn^{II}Cr^{III}$ and $Ni^{II}Cr^{III}$ chloride lattices in their ground AF, FO and FO states respectively.

F_0	a_0	K_0	d_{M-Cl}	d'_{M-Cl}	d_{Cr-Cl}	d'_{Cr-Cl}
$V^{II}Cr^{III}$ (AF ground state)						
35	9.937	39.62	2.566	−24.5	2.403	−13.9
65	9.890	42.39	2.559	−24.4	2.386	−12.9
100	9.841	45.51	2.548	−23.8	2.373	−12.3
UHF	10.142	35.79	2.639	−27.6	2.432	−14.1
$Mn^{II}Cr^{III}$ (FO ground state)						
35	9.961	39.76	2.574	−24.9	2.407	−14.1
65	9.914	42.56	2.570	−24.5	2.387	−12.8
100	9.862	45.57	2.557	−22.3	2.374	−12.0
UHF	10.160	35.97	2.647	−28.2	2.433	−13.9
$Ni^{II}Cr^{III}$ (FO ground state)						
35	9.783	43.81	2.484	−20.8	2.408	−13.9
65	9.736	46.89	2.480	−19.4	2.388	−13.9
100	9.688	50.32	2.469	−19.4	2.375	−11.5
UHF	9.982	39.18	2.556	−24.1	2.435	−13.8

$Mn_3[Cr(CN)_6]_2{\cdot}16H_2O$ [16]. We note however that the experimental structure differs notably from the model we have used here, in that the latter incorporates K^I counterions at one-half of the available tetrahedral sites, possesses completely occupied TM and ligand sublattices, and omits disordered water molecules. The present results offer no insight into whether the disparities in elastic properties are due to these differences in crystal structure and composition, or to a more fundamental deficiency in the theoretical methods applied. The likelihood of the latter explanation is reduced by the fact that hybrid functionals have been shown to provide bulk moduli in good agreement with experimental values in a wide range of TM compounds [27, 42]. Further investigation of this point must await theoretical studies of more realistic lacunary PBA structures incorporating $M^{III}(CN)_6$ vacancies and hydration. We note also that the chloride bulk moduli are all in a range from 1 to 5 GPa below the values for the corresponding cyanide, the similarity in the parameters suggesting that the ionic interactions are of comparable strength in both sets of compounds.

The response of the structures to pressure is of fundamental interest, for we expect the magnetic coupling to be significantly enhanced by even the most modest reductions in intersite distances. We find that the M^{II}–N (and M^{II}–Cl) bonds are the most compressible, with a rate of change of length with pressure (d') that is approximately 1.5 times–(1.8 times in the chlorides) larger than the Cr^{III}–C (and Cr^{III}–Cl) bonds. The C≡N covalent bonds, by way of contrast, remain largely unaffected by lattice compression, shortening at rates that are at least an order of magnitude lower than the ionic bonds. The Cr^{III}–C and Cr^{III}–Cl bonds show a similar rate of compression in all compounds and Hamiltonians, despite the fact that the latter are approximately 0.3 Å longer than the former. The (V^{II}, Mn^{II})–N bonds compress more rapidly than the Ni^{II}–N bond, and similarly, the (V^{II}, Mn^{II})–Cl bonds more rapidly than the Ni^{II}–Cl bond. Furthermore, we note that the (V^{II}, Mn^{II}, Ni^{II})–Cl bonds are more compressible than the (V^{II}, Mn^{II}, Ni^{II})–N bonds, in keeping with the slightly lower bulk moduli obtained in the chlorides.

3.2. Charges

Tables 3 (cyanides) and 4 (chlorides) present the Mulliken atomic charges (q), spin moments (μ), valence-to-conduction band energy gap widths (ΔE_g), and atomic compositions of the valence (VBE) and conduction band edge (CBE) states obtained within the ground magnetic states of the six compounds at equilibrium. Direct comparisons of the absolute charges are hampered by the difficulties discussed in section 2 above, but we take from the results evidence for a tendency toward charges at V and Cr sites that are lower, relative to the respective formal values, than the comparable Mn and Ni charges. The $F_0 = 35\%$ overlap populations offer some insight into this observation, yielding values for the (V, Cr, Mn, Ni)–ligand bonds of (0.062, 0.057, 0.011 and 0.019) e respectively in the cyanides, and (0.040, 0.048, 0.017 and 0.015) e respectively in the chlorides. An increased covalency is therefore apparent in the bonds involving V and Cr ions, which may be attributed to the well-known tendency towards more diffuse d-orbitals in the early TM ions [44]. The trends in the ligand charges across the range of materials also support this interpretation, revealing values in the $V^{II}Cr^{III}$ cyanide and chloride that are lower than in the comparable $Mn^{II}Cr^{III}$ and $Ni^{II}Cr^{III}$ systems. The variations in the $F_0 = 35\%$ dynamical charges across the three PBAs follow a similar pattern, in that we obtain Cr and V values lying well below the respective formal values, whereas the Mn and Ni charges are substantially higher, and in fact exceed the respective formal values. Moreover, the summed C and N dynamical charges are, again, lower in the $V^{II}Cr^{III}$ PBA than in either of the $Mn^{II}Cr^{III}$

Table 3. The variation with Fock exchange content (F_0) in the summed ligand Mulliken charges, q(CN) (e), metal charges, q(Cr) and q(M) (e) (D denotes dynamical charge), Mulliken spin moments μ(N), μ(C), μ(Cr), μ(M) and μ (cell) (μ_B), valence-to-conduction band gaps, ΔE_g (eV), and relative valence—(VBE) and conduction band edge (CBE) compositions, w (%) for the equilibrium $V^{II}Cr^{III}$, $Mn^{II}Cr^{III}$ and $Ni^{II}Cr^{III}$ cyanide lattices in their ground AF, FI and FO states respectively.

F_0	q(CN)	q(Cr)	q(M)	μ(N)	μ(C)	μ(Cr)	μ(M)	μ(cell)	ΔE_g	VBE w_{CN}, w_{Cr}, w_M	CBE w_{CN}, w_{Cr}, w_M
					$V^{II}Cr^{III}$ (AF ground state)						
35	−0.701	1.850	1.377	−0.149	0.173	−2.989	2.842	−0.003	4.01	13 0, 87	45, 51, 4
	-0.790^D	2.070^D	1.528^D								
65	−0.728	1.954	1.430	−0.146	0.167	−3.070	2.946	0.002	7.84	13, 0, 87	62, 38, 1
100	−0.756	2.067	1.479	−0.153	0.169	−3.083	2.984	−0.003	12.21	17, 0, 83	67, 33, 0
UHF	−0.784	2.139	1.580	−0.238	0.259	−3.160	3.034	0.000	12.94	20, 0, 79	69, 30, 1
					$Mn^{II}Cr^{III}$ (FI ground state)						
35	−0.756	1.852	1.704	−0.083	0.112	−2.997	4.821	1.998	5.84	40, 0, 60	50, 49, 1
	-0.932^D	1.779^D	2.771^D								
65	−0.779	1.955	1.737	−0.081	0.113	−3.065	4.870	1.997	9.94	54, 1, 45	60, 40, 1
100	−0.803	2.068	1.763	−0.084	0.114	−3.076	4.896	2.000	14.24	98, 0, 4	68, 32, 1
UHF	−0.824	2.141	1.813	−0.146	0.181	−3.147	4.941	2.004	14.56	93, 0, 6	71, 29, 1
					$Ni^{II}Cr^{III}$ (FO ground state)						
35	−0.762	1.856	1.740	0.138	−0.108	3.014	1.806	5.000	6.95	75, 5, 20	51, 48, 1
	-0.895^D	1.856^D	2.406^D								
65	−0.788	1.958	1.789	0.126	−0.117	3.075	1.873	5.002	10.60	93, 1, 6	59, 41, 1
100	−0.812	2.069	1.820	0.130	−0.128	3.084	1.908	5.004	14.34	100, 0, 0	68, 31, 1
UHF	−0.831	2.143	1.855	0.194	−0.208	3.154	1.931	5.001	14.43	100, 0, 0	71, 28, 1

Table 4. The variation with Fock exchange content (F_0) in the ligand, q(Cl), and metal Mulliken charges, q(Cr) and q(M) (e), Mulliken spin moments μ(Cl), μ(Cr), μ(M) and μ (cell) (μ_B), valence-to-conduction band gap, ΔE_g (eV), and relative valence—(VBE) and conduction band edge (CBE) compositions, w (%) for the equilibrium $V^{II}Cr^{III}$, $Mn^{II}Cr^{III}$ and $Ni^{II}Cr^{III}$ chloride lattices in their ground AF, FO and FO states respectively.

F_0	q(Cl)	q(Cr)	q(M)	μ(Cl)	μ(Cr)	μ(M)	μ(cell)	ΔE_g	VBE w_{Cl}, w_{Cr}, w_M	CBE w_{Cl}, w_{Cr}, w_M
					$V^{II}Cr^{III}$ (AF ground state)					
35	−0.706	1.835	1.414	0.019	−3.113	3.003	0.004	3.43	33, 0, 67	18, 62, 20
65	−0.744	1.970	1.502	0.017	−3.099	3.000	0.003	7.18	57, 0, 43	19, 75, 6
100	−0.780	2.111	1.570	0.011	−3.057	2.994	0.003	11.11	84, 0, 16	16, 78, 6
UHF	−0.806	2.181	1.655	0.018	−3.135	3.029	0.002	10.64	100, 0, 0	20, 80, 0
					$Mn^{II}Cr^{III}$ (FO ground state)					
35	−0.746	1.833	1.652	0.000	3.196	4.802	7.998	4.02	99, 0, 1	24, 74, 2
65	−0.779	1.967	1.717	−0.002	3.147	4.864	7.999	7.01	100, 0, 0	23, 76, 1
100	−0.811	2.107	1.760	0.003	3.086	4.894	7.998	10.99	99, 0, 1	21, 78, 1
UHF	−0.832	2.180	1.814	−0.013	3.143	4.933	7.998	10.41	100, 0, 0	21, 78, 1
					$Ni^{II}Cr^{III}$ (FO ground state)					
35	−0.755	1.847	1.689	0.004	3.192	1.781	4.997	3.73	100, 0, 0	24, 75, 1
65	−0.794	1.984	1.784	−0.004	3.145	1.880	5.001	6.67	100, 0, 0	23, 76, 1
100	−0.827	2.126	1.835	−0.001	3.083	1.924	5.001	10.61	100. 0, 0	20, 79, 1
UHF	−0.844	2.194	1.870	−0.015	3.145	1.944	4.999	10.22	100, 0, 0	20, 79, 1

or $Ni^{II}Cr^{III}$ systems. The K charges obtained from both the Mulliken and dynamical analyses remain close to $+1|e|$ across the range of materials and Hamiltonians. Finally, we find that the Mulliken charges increase in magnitude as F_0 is raised in all cases, indicating that, as in the TMOs [26, 27, 42], Hamiltonians with larger contents of Fock exchange produce more ionic ground states.

We turn now to examine the variations in the Mulliken charges with increase in pressure to a maximum of approximately 15 GPa. The discussion is simplified by presenting the pressure derivatives of the charges (q') obtained from the $F_0 = 35\%$ calculations alone, with the knowledge that the other Hamiltonians yield similar results, and we note that the rates of change must be interpreted relative to

the absolute charges established at equilibrium. Reporting first upon values common to a number of materials, we find that the rate q'(Cr) varies within a narrow range from -0.0108 to $-0.0137|e|$ GPa^{-1} across all of the compounds, while q'(C) varies from $+0.0019$ to $+0.0027|e|$ GPa^{-1} within the cyanides. More substantial differences are apparent in the pressure derivatives of the V, Mn and Ni charges, with values of -0.0253, -0.0127 and $-0.0065|e|$ GPa^{-1} respectively emerging in the cyanides, and similar in the chlorides. The q' values for the N and Cl atoms correlate with those of the neighbouring M^{II} site, varying from $+0.0010$ to $+0.0042|e|$ GPa^{-1} in the cyanides, and from $+0.0033$ to $+0.0058|e|$ GPa^{-1} in the chlorides. Finally, we note that the pressure derivatives for a given M^{II} ion obey the relationship $q'(\mathrm{Cl}) \approx q'(\mathrm{C}) + q'(\mathrm{N})$, indicating that, regardless of the differences in their compositions, the net charges borne by the ligands vary in an essentially identical fashion with pressure.

3.3. Spin moments

The Mulliken spin moments borne by the V^{II}, Mn^{II} and Ni^{II} ions do not vary far from their ideal, spin-only values of 3, 5 and 2 μ_B respectively in any of the compounds studied. The Cr^{III} moments also remain close to the ideal value of 3 μ_B, and are in fact often found to exceed it, despite our earlier observations of reduced ionic charges at these sites. A decomposition of the Cr population into orbital contributions offers further insight, yielding total e_g- and t_{2g}-orbital occupations in the $Mn^{II}Cr^{III}$ cyanide at $F_0 = 35\%$ of 1.11 and 2.90e respectively, and spin-polarized occupations of -0.18 and -2.82 μ_B respectively, with similar values arising in other Hamiltonians and materials. Thus, we see immediately that the low charges and large spin moments at Cr sites arise out of the partially spin-paired occupation of the e_g-orbitals. The TM moments increase in magnitude as F_0 is raised, which again supports the notion that Hamiltonians incorporating larger admixtures of Fock exchange produce more ionic ground states.

Turning to examine the ligand spin densities, we note first that the Cl sites bear only small net polarizations, in keeping with our expectations for a single ion superexchange bridge. The cyanide C and N atoms, by way of contrast, bear comparatively large, counter-aligned moments in all cases. In particular, we see that the C moments align anti-parallel to the Cr^{III} spins in both magnetic states of all three PBAs, suggestive of a particularly large overlap between the singly-occupied orbitals upon these two sites. The magnitudes of the C and N moments do not vary greatly with Fock exchange content, save at the transition from the $F_0 = 100\%$ to UHF Hamiltonians wherein the removal of the LYP correlation functional leads to marked increases in all three materials.

Figure 2 shows the projections onto the conventional (100) plane of the $F_0 = 35\%$ spin densities in the FI and FO states of the $Mn^{II}Cr^{III}$ cyanide and chloride, along with corresponding plots for the CN^--isomerized lattice. Detailed examinations verify the conclusions drawn from the Mulliken analyses, and show that the spin density borne by the CN^- ligands resides in both π- and lone pair orbitals, whereas only very small σ-orbital polarizations are evident at Cl^- sites. Interestingly, the $Mn^{II}Cr^{III}$ PBA plots also provide some evidence for a partial decoupling of the ligand spin density from the underlying crystal structure, revealing distributions of similar form in both isomerized states of the lattice. We note, though, that isomerization does affect the strength of the magnetic coupling in all three PBAs, as discussed in section 3.6 below.

As for the bond lengths and charges, the variations in the spin moments with pressure are of fundamental interest. Again, we present only the $F_0 = 35\%$ values, on the basis that the trends in the other Hamiltonians are similar. Examining the TM sites first, we find rates of change in the magnitude of the Cr^{III} moment with pressure ($|\mu|'$), ranging from -0.012 to -0.018 μ_B GPa^{-1} across the cyanides, and from -0.005 to -0.010 μ_B GPa^{-1} in the chlorides, while the comparable values for the V^{II}, Mn^{II} and Ni^{II} moments are -0.021, -0.014 and -0.006 μ_B GPa^{-1} respectively in the cyanides, and -0.003, -0.010 and -0.006 μ_B GPa^{-1} respectively in the chlorides. The decline in TM moments with lattice compression can be attributed to the increase in crystal field splitting, favouring spin-paired occupation of the t_{2g}-orbitals; and to the enhancement in the strength of the ligand electron screening, which weakens the intra-atomic exchange interactions and increases the effective d-orbital radii. We note, however, that the screening-derived effects are unlikely to contribute significantly to the differences apparent in the cyanides and chloride TM $|\mu|'$ values, given that the nephelauxetic factors of the CN^- and Cl^- ligands are similar, at 2.1 and 2.0 respectively [45]. Rather, we suggest that the larger $|\mu|'$ values obtained in the cyanides arise out of the fact that the CN^- ligand is spectrochemically stronger than Cl^- [46]. Finally we examine the variation with pressure in the net polarizations $|\mu(\mathrm{C})–\mu(\mathrm{N})|$ of the CN^- ligands, obtaining values of $+0.012$, $+0.008$ and $+0.006$ μ_B GPa^{-1} in the $V^{II}Cr^{III}$, $Mn^{II}Cr^{III}$ and $Ni^{II}Cr^{III}$ cyanides respectively. The increasing trend is common to all Hamiltonians, and may be attributed to the progressive enhancement in metal–ligand orbital overlap as the bonds shorten.

3.4. Electronic structure and densities-of-states

The compositions of the valence- (VBE) and conduction band edge (CBE) states are presented in tables 3 and 4, while figure 3 shows the $F_0 = 35\%$ densities-of-states plots for the compounds within their respective ground magnetic states. The states have been partitioned into separate contributions due to the M^{II}, Cr^{III} and ligand sublattices via the Mulliken method. Examining the PBA results first, we find CBEs composed of relatively equal weights of ligand- and Cr-derived states; the contribution due to the former growing as F_0 is increased. The VBE weightings, by way of contrast, are much more sensitive to crystal composition, varying from domination by V-derived states in the V^{II} compound, to CN-derived states in the Ni^{II} lattice. The VBE of the Mn^{II} cyanide is of particular interest, displaying a crossover from a majority of Mn-derived states at low F_0 to CN-derived states as Fock exchange content increases. Similar trends are apparent in the VBE compositions of the V^{II} and Ni^{II} compounds, but in neither of these cases do they suffice to

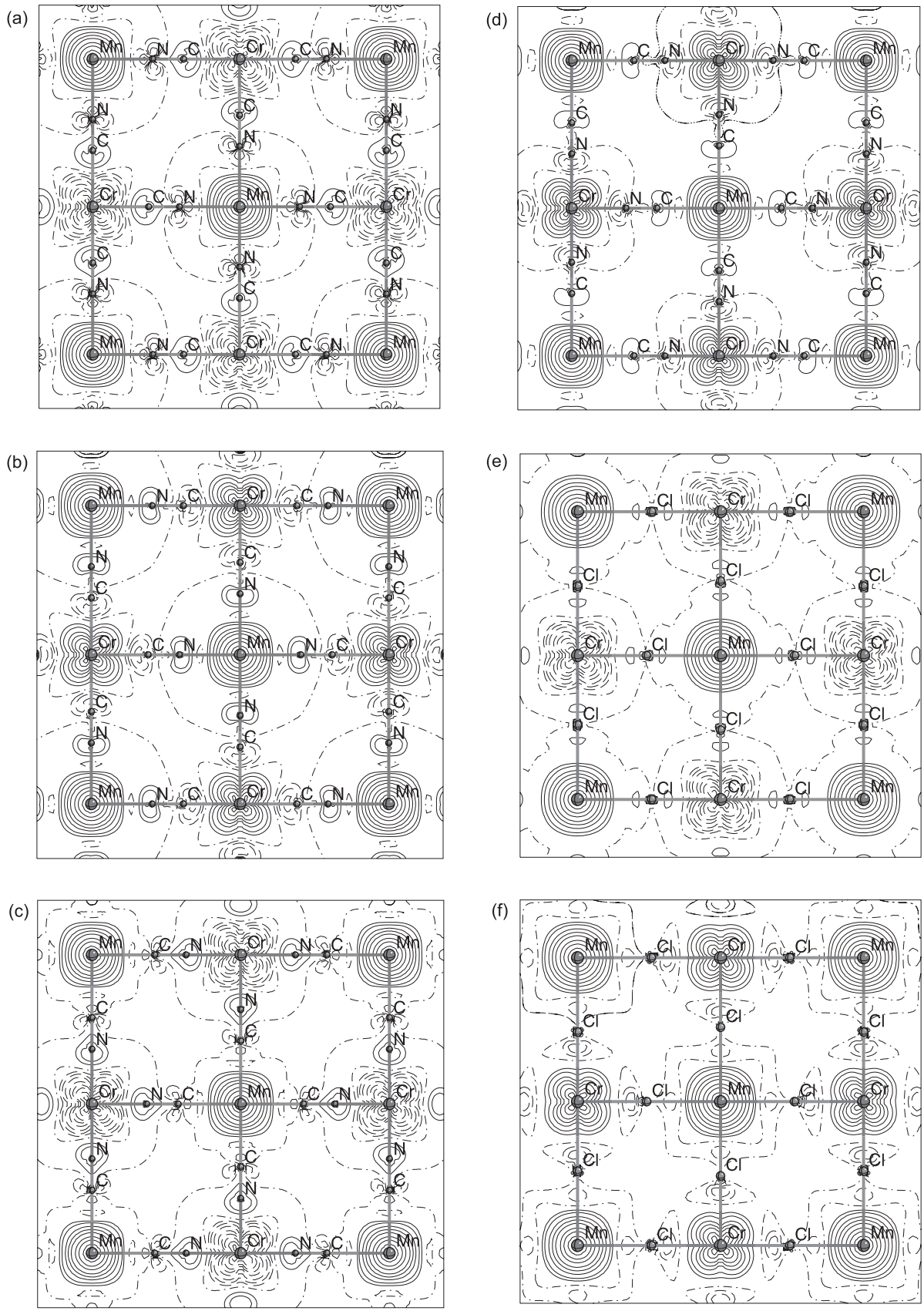

Figure 2. The spin densities at $F_0 = 35\%$ in the (100) planes of the $Mn^{II}Cr^{III}$ materials, plotted on a logarithmic scale for (a) FI and (b) FO orders with low energy CN isomerization, (c) FI and (d) FO orders with high energy CN isomerization, (e) FI and (f) FO orders in the chloride. Solid, dashed and dot–dashed contours indicate positive, negative and zero spin density respectively.

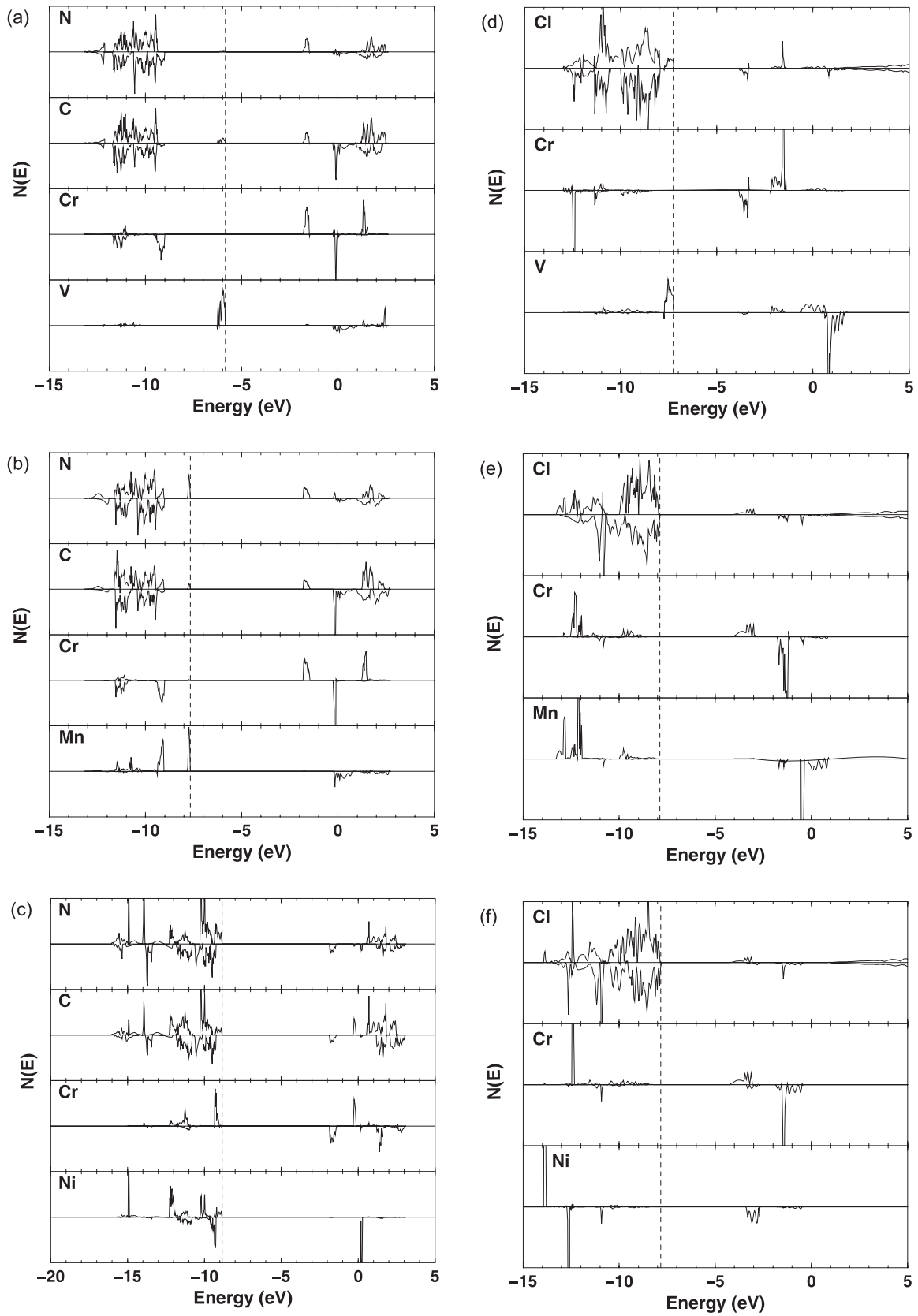

Figure 3. Atom-projected densities-of-states plots at equilibrium for (a) AF $V^{II}Cr^{III}$, (b) FI $Mn^{II}Cr^{III}$ and (c) FO $Ni^{II}Cr^{III}$ cyanides, and (d) AF $V^{II}Cr^{III}$, (e) FO $Mn^{II}Cr^{III}$ and (f) FO $Ni^{II}Cr^{III}$ chlorides for $F_0 = 35\%$. Positive values in each pane show α-spin states, negative show β-states. Vertical dashed lines indicate the positions of the valence band edges.

alter the character of the band edge. Previous studies of the TMOs also found a general tendency toward the domination of the VBEs by metal states at low F_0 values and ligand states at high F_0 [26, 27]. The effect was attributed to the progressive weakening in the TM d-orbital self-interactions with increasing Fock exchange content, leading to a stabilization of the filled metal states relative to the anion bands [26, 27]. It is reasonable to suggest that a similar mechanism operates in the current compounds. Moreover, the variation in VBE character across the range of M^{II} cations is qualitatively similar to previous observations in the TMOs [26, 27]. The CBEs of the chlorides possess significantly higher weights of Cr-derived states than the cyanides, with correspondingly lower weights of ligand-derived states. Again, we note that the VBE characters vary markedly with composition: V- and Cl-derived states dominating at low and high values of F_0 respectively in the V^{II} compound, while the VBEs of the Mn^{II} and Ni^{II} lattices derive almost exclusively from ligand states.

We note in passing that the electronic structure of the aliovalently-doped phases may be inferred from these results; the electron hole and addition states of the various lattices adopting characters determined by the VBE and CBE compositions respectively. To this end, we mention also the conclusion of a previous study of the trapped holes in MgO:$[Li]^0$, namely that an F_0 value of approximately 30% yielded the best overall agreement between the computed and experimental hyperfine and nuclear quadrupole coupling constants [27]. We suggest on this basis that the hole characters inferred from the current $F_0 = 35\%$ calculations may be taken as representative. Further statements as to the degree of localization of the electronic defects must await direct supercell calculations, although we note that hole localization is more favoured the narrower in energy the valence bands bordering the gap become, while the addition states are likely to be delocalized.

We also examine the width of the gaps, ΔE_g, separating the valence and conduction bands, as presented in tables 3 and 4. It is clear that ΔE_g increases with F_0 in each compound, with plots of the data (not shown) indicating near linear dependencies. Extrapolations permit the estimation of the band gaps within the $F_0 = 20\%$ (B3LYP) Hamiltonian, which previous studies have shown provides values in good agreement with experiment within a wide variety of compounds [47]. On this basis, we predict band gaps of width 2.1, 4.0 and 5.3 eV in the V^{II}, Mn^{II} and Ni^{II} PBAs respectively, and of width 1.7, 2.3 and 2.1 eV in the chlorides respectively. The characters of the excitations follow from the respective VBE and CBE compositions discussed above. However, a note of caution is in order here, for excitations involving highly localized states may entail extensive band relaxations, effectively ruling out simple interpretations based upon a rigid band model of the sort discussed here. Finally, we note that the all of the gaps narrow with increasing pressure; the $\partial(\Delta E_g)/\partial P$ value of -0.24 eV GPa^{-1} obtained in the $Mn^{II}Cr^{III}$ cyanide being quite generally representative of these trends.

3.5. Magnetic coupling

The energies per TM site of the FO and FI (or AF) states may be derived from the nearest-neighbour Ising Hamiltonian (2) as

$$E[\mathrm{FM}] = E_0 + 3J\bar{S}^2, \qquad E[\mathrm{AF, FI}] = E_0 - 3J\bar{S}^2, \tag{6}$$

where E is the energy of the putative non-magnetic lattice and $\bar{S}^2 = \sqrt{S_{\mathrm{II}}(S_{\mathrm{II}}+1)S_{\mathrm{III}}(S_{\mathrm{III}}+1)}$; S_{II} and S_{III} representing the spin moments borne by ions upon the M^{II} and Cr^{III} sublattices respectively. Positive values of J favour the AF (or FI) ground state within this sign convention. The coupling constants are straightforwardly determined from the differences in the calculated total energies of the FO and AF (or FI) states as

$$J = \frac{E\,[\mathrm{FM}] - E\,[\mathrm{AF\ or\ FI}]}{6\bar{S}^2}, \tag{7}$$

while their volume dependencies are obtained from a series of calculations at varying lattice constants. All of our subsequent analyses use the ideal, spin-only values $S_{\mathrm{II}} = 3/2$, $5/2$ and 1, and $S_{\mathrm{III}} = 3/2$ for the V^{II}, Mn^{II}, Ni^{II} and Cr^{III} cations respectively. As in the previous cluster calculations of Ruiz *et al* [19], we estimate the critical temperature for the transition from spin order to paramagnetism within the mean field approach of Langevin, Weiss and Néel [48], obtaining

$$T_{\mathrm{C}} = \frac{6\,|J|\,\bar{S}^2}{3k_{\mathrm{B}}}. \tag{8}$$

We note that the magnetic energy differences separating the ordered states at equilibrium range from a minimum of $0.17mE_{\mathrm{h}}$ for the $Mn^{II}Cr^{III}$ PBA in the UHF method to a maximum of $3.64mE_{\mathrm{h}}$ for the $V^{II}Cr^{III}$ PBA at $F_0 = 35\%$. It is clear, therefore, that our total energy convergence tolerance of $0.1\mu E_{\mathrm{h}}$ provides adequate precision in the calculated coupling constants.

Tables 5 and 6 present the ground magnetic states, coupling constants and estimated critical temperatures for the cyanides and chlorides respectively. We find that the characters of the ground states are in agreement with the qualitative analysis advanced in section 1, most notably in that the sign and magnitude of the coupling in the $Mn^{II}Cr^{III}$ compounds varies from weakly AF in the PBA to strongly FO in the chloride. Similarly, the AF ground state of the $V^{II}Cr^{III}$ PBA is more stable with respect to disorder than that of the corresponding chloride, while the opposite trend prevails for the FO ground states of the $Ni^{II}Cr^{III}$ compounds. The estimated T_{C} obtained for the $V^{II}Cr^{III}$ cyanide from the optimal magnetic $F_0 = 35\%$ method [25] exceeds the comparable experimental value [6] by approximately 2%, while the similarly determined T_{C} in the $Ni^{II}Cr^{III}$ cyanide underestimates experiment [49] by approximately 2%. We note, however, that direct comparisons of the theoretical and experimental T_{C} values are hampered by the presence of low concentrations of V^{II} impurities and hydration in samples of the former material [6], and by the presence of Cs rather than K counterions in the latter [49].

Significantly poorer agreement emerges for the experimental and theoretical critical temperatures in the $Mn^{II}Cr^{III}$

Table 5. The variation with Fock exchange content (F_0) in the magnitudes of the magnetic coupling constants, $|J|$ (K), estimated critical temperatures, T_C (K), and magnetic Grüneisen constants obtained from cubic, ε_c, and linear fits, ε_l, to $\ln(\Delta E_{mag})$–$\ln V$ plots for the equilibrium (a_0) $V^{II}Cr^{III}$, $Mn^{II}Cr^{III}$ and $Ni^{II}Cr^{III}$ cyanide lattices. Comparable experimental T_C and ε values are from (1) $KV[Cr(CN)_6]\cdot 2H_2O$ [6], (2) $CsMn[Cr(CN)_6]$ [50], (3) $Mn_3[Cr(CN)_6]_2\cdot 16H_2O$ [16], (4) $CsNi[Cr(CN)_6]\cdot 2H_2O$ [49].

F_0	$\lvert J\rvert/k_B$	T_C	$\varepsilon_c(a_0)$	ε_l
$V^{II}Cr^{III}$ (AF ground state)				
35	51.08	383.1	6.34	6.24
65	27.83	208.8	6.33	6.19
100	20.21	151.6	6.14	6.06
UHF	23.65	177.4	5.25	5.16
Expt.	—	376[1]	—	—
$Mn^{II}Cr^{III}$ (FI ground state)				
35	4.46	51.2	9.22	8.48
65	2.47	28.4	9.78	8.83
100	1.45	16.7	12.07	10.43
UHF	1.56	17.9	9.91	8.56
Expt.	—	90[2], 59[3]	9.96[3]	
$Ni^{II}Cr^{III}$ (FO ground state)				
35	16.17	88.6	4.29	4.32
65	11.82	64.7	4.46	4.49
100	10.67	58.4	4.51	4.50
UHF	13.98	76.6	4.04	4.00
Expt.	—	90[4]	—	—

cyanide. The comparable experimental values in this case are 90 and 59 K, as obtained from $CsMn[Cr(CN)_6]$ [50] and $Mn_3[Cr(CN)_6]_2\cdot 16H_2O$ [16] respectively. We suggest that the latter value should be multiplied by a stoichiometry-derived factor

$$\frac{6}{\sqrt{x Z^{II} Z^{III}}} = \frac{3}{2}, \tag{9}$$

prior to comparison with theory, where x denotes the stoichiometry $M^{II}[M^{III}(CN)_6]_x$; and Z^{II} and Z^{III}, the average magnetic coordination of ions upon the respective sublattices; yielding a T_C of 89 K for the notionally 'ideal' lattice. Thus, the estimated T_C value at $F_0 = 35\%$ underestimates the adjusted experimental range (89–90 K) by approximately 43%. The discrepancy may be due to the overestimation of the theoretical lattice constant, to the inaccurate representation of the relative strengths of FO and AF contributions, or to some combination of both effects.

Tables 5 and 6 also present the magnetic Grüneisen constants, ε, obtained from linear (l) and cubic (c) fits to plots of $\ln(\Delta E_{Mag})$ against $\ln(V)$. The values reported for the cubic fits are those obtained at structural equilibrium (a_0). Representative curves for the $Mn^{II}Cr^{III}$ PBA and chloride are shown in figures 4 and 5 respectively. In general we find that the ε values obtained from the linear and cubic functions are very similar, indicating that Bloch's relationship (1) provides an accurate description of the magnetism in these compounds across a wide range of pressures. However, the $Mn^{II}Cr^{III}$ PBA results emerge as a clear exception, yielding $\varepsilon_c(a_0)$ and ε_l values that differ markedly. Figure 4 reveals

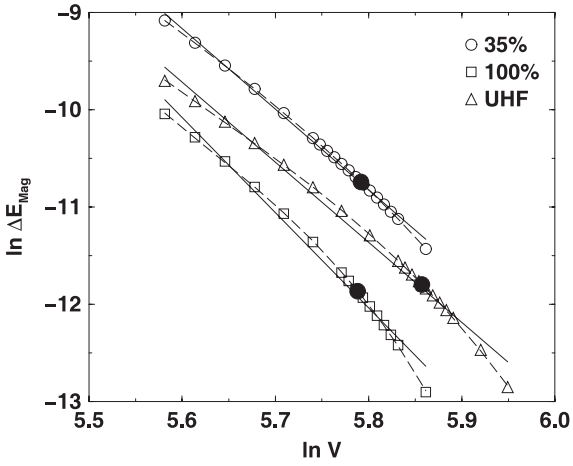

Figure 4. Plots of the logarithm of the difference in energy between FO and FI orders, $\ln(\Delta E_{Mag})$, against the logarithm of the cell volume, $\ln(V)$, in the $Mn^{II}Cr^{III}$ cyanide for varying values of F_0. Filled circles denote values at equilibrium, solid lines show linear fits, dashed lines show cubic fits.

Table 6. The variation with Fock exchange content (F_0) in the magnitudes of the magnetic coupling constants, $|J|$ (K), estimated critical temperatures, T_C (K), and magnetic Grüneisen constants obtained from cubic, ε_c, and linear fits, ε_l, to $\ln(\Delta E_{mag})$–ln V plots for the equilibrium (a_0) $V^{II}Cr^{III}$, $Mn^{II}Cr^{III}$ and $Ni^{II}Cr^{III}$ chloride lattices.

F_0	$\lvert J\rvert/k_B$	T_C	$\varepsilon_c(a_0)$	ε_l
$V^{II}Cr^{III}$ (AF ground state)				
35	10.85	81.4	3.70	3.66
65	7.61	57.1	4.04	4.16
100	5.32	39.9	4.68	4.99
UHF	6.50	48.7	3.33	3.33
$Mn^{II}Cr^{III}$ (FO ground state)				
35	15.67	179.5	1.86	1.95
65	10.19	116.7	2.12	2.28
100	6.37	73.0	2.58	2.79
UHF	5.75	65.9	3.09	2.98
$Ni^{II}Cr^{III}$ (FO ground state)				
35	39.07	214.0	1.65	1.65
65	25.03	137.1	2.33	2.41
100	15.33	84.0	3.10	3.28
UHF	14.65	80.3	3.26	3.20

that the gradients of the $\ln(\Delta E_{Mag})$–$\ln(V)$ curves in this material vary substantially across the volume range, which implies that a simple relationship of the Bloch form (1) is not applicable. Alternatively, ε may itself be viewed as a volume-dependent quantity, an effect that we attribute to the fact that the AF and FO contributions to the net coupling are likely to scale at different rates with distance. In terms of magnitude, we find values in the $V^{II}Cr^{III}$ and $Ni^{II}Cr^{III}$ PBAs notably in excess of the range 3–4 established previously for the TM oxides and fluorides [11–15], $Mn^{II}Cr^{III}$ PBA values that are larger still, and chloride values falling within or slightly below that range. While the exponents obtained for all three PBAs may be considered high, we

Table 7. The energies relative to the optimized $F_0 = 35\%$ structures of lattices in which every ligand has been isomerized, for both high- and low-spin Mn^{II} configurations, ΔE_{CN}^{HS} (Full) and ΔE_{CN}^{LS} (Full); and in which one ligand in six has been isomerized, ΔE_{CN}^{HS} (1-in-6). Also shown are the factors multiplying the magnetic interaction strengths in the fully isomerized lattices, M, and the relevant bond lengths, d (Å) around the isomerized ligands in the fully isomerized and 1-in-6 structures. Energies are in meV per isomerized CN ligand.

					Full lattice			1-in-6 lattice		
Material	ΔE_{CN}^{HS} (Full)	ΔE_{CN}^{LS} (Full)	ΔE_{CN}^{HS} (1-in-6)	M	d_{C-N}	d_{M-C}	d_{Cr-N}	d_{C-N}	d_{M-C}	d_{Cr-N}
$V^{II}Cr^{III}$ (AF)	42.6	—	78.6	0.86	1.155	2.188	2.023	1.155	2.183	2.017
$Mn^{II}Cr^{III}$ (FI)	143.1	365.1	150.1	0.47	1.153	2.307	2.012	1.153	2.301	2.020
$Ni^{II}Cr^{III}$ (FO)	46.8	—	69.1	1.26	1.153	2.147	2.023	1.153	2.117	2.025

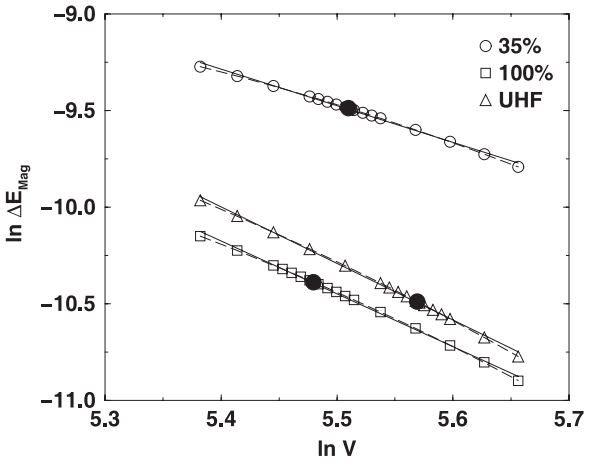

Figure 5. Plots of the logarithm of the difference in energy between FO and FI orders, $\ln(\Delta E_{Mag})$, against the logarithm of the cell volume, $\ln(V)$, in the $Mn^{II}Cr^{III}$ chloride for varying values of F_0. Filled circles denote values at equilibrium, solid lines show linear fits, dashed lines show cubic fits.

conclude that it is only the $Mn^{II}Cr^{III}$ compound that displays the extreme magnetostructural correlations observed within the previous study [16]. Further investigations of PBAs incorporating competing FO and AF interactions are expected to be revealing, and we are now undertaking a similar study of the mixed-valent $Cr^{II}Cr^{III}$ system at pressure.

3.6. Ligand isomerism

Isomerized CN^- ligands will be present as lattice defects at low concentrations in all PBAs, but previous studies indicate their particular prevalence in the $Ni^{II}Cr^{III}$-based PBAs [49, 51], with affect upon the magnetism and structural stability of the lattice. Crystals of $CsNi^{II}[Cr^{III}(CN)_6]\cdot 2H_2O$ have been observed to undergo a change of colour from grey to yellow over the course of a few days following synthesis, which is believed to be due to a progressive increase in the concentration of square–planar, diamagnetic $Ni^{II}(CN)_4$ centres [49, 51]. Such processes are known to be governed by the change in the crystal field stabilization energies (CFSE) of the TM cations neighbouring the flipped ligands [5], but quantitative estimates of the energies involved are apparently lacking in the literature. Our subsequent analysis adopts the notation $\Delta^{A,B}$ to denote the crystal field splitting energy of the B TM cation arising from its proximity to the A atom of the CN^- ligand. The isomerization-induced changes in the total CFSEs per formula unit of the three compounds may then be written

$$\begin{aligned} V^{II}Cr^{III}\text{:}\quad & \Delta E_{CFSE} = \tfrac{6}{5}\left(\Delta^{N,V} + \Delta^{C,Cr} - \Delta^{N,Cr} - \Delta^{C,V}\right) \\ Mn^{II}Cr^{III}\text{:}\quad & \Delta E_{CFSE} = \tfrac{6}{5}\left(\Delta^{C,Cr} - \Delta^{N,Cr}\right) \\ Ni^{II}Cr^{III}\text{:}\quad & \Delta E_{CFSE} = \tfrac{6}{5}\left(\Delta^{N,Ni} + \Delta^{C,Cr} - \Delta^{N,Cr} - \Delta^{C,Ni}\right). \end{aligned} \tag{10}$$

The strong field $\Delta^{C,B}$ splittings will be larger than the comparable weak field $\Delta^{N,B}$ terms, and so ΔE_{CFSE} is predicted be higher in the $Mn^{II}Cr^{III}$ PBA than in either $V^{II}Cr^{III}$ or $Ni^{II}Cr^{III}$. Experimental studies support this qualitative model, finding no apparent isomerized ligands in $CsMn^{II}[Cr^{III}(CN)_6]$ [50], whereas they are known to be common in $CsNi^{II}[Cr^{III}(CN)_6]\cdot 2H_2O$, as discussed above.

Our $F_0 = 35\%$ calculations consider two isomerized structures: the first in which all six CN^- ligands in the primitive cell are reversed; and the second, reduced symmetry case in which only one ligand is reversed. The atomic positions in the isomerized lattices have been re-optimized, with cell constants fixed at the respective ground state equilibrium values. Both high-spin (HS) $e_g^2t_{2g}^3$ and low-spin (LS) t_{2g}^5 Mn^{II} configurations have been considered, the latter represented in a cell in which the equivalence of the (xz, yz)- and xy-orbitals was removed by application of an infinitesimal tetragonal distortion. The computed isomerization energies are presented in table 7, along with the relevant bond lengths within and around the reversed ligands and the factor, M, multiplying the magnetic interaction strengths in the fully isomerized lattices. We find that the isomerization energy of the $Mn^{II}Cr^{III}$ lattice is approximately three times larger than the $V^{II}Cr^{III}$ and $Ni^{II}Cr^{III}$ values, confirming the results of the qualitative CFSE model. The LS Mn^{II} state is of sufficiently high energy that it need not be considered further. We note also that the energy required to effect a single isomerization is significantly higher than the energy per ligand of the fully isomerized lattice in all three materials, suggestive of a strong tendency toward the formation of isomerized domains. Interestingly, we note that linkage isomerization weakens the exchange coupling in the $V^{II}Cr^{III}$ and $Mn^{II}Cr^{III}$ PBAs, but leads to an enhancement in the $Ni^{II}Cr^{III}$ compound.

4. Conclusions

The current paper reports upon a comprehensive study of the structural, electronic and magnetic properties of three

PBAs and associated chlorides at pressure. The use of a range of hybrid functionals has permitted us to draw quite general conclusions regarding the computed properties. Our primary conclusion is that while all three PBAs display large Bloch exponents (ε, equation (1)), the extremely strong magnetostructural correlations observed in the $Mn^{II}Cr^{III}$ system [16] are not a property of such materials in general. The additional findings are:

(i) Variation in the Fock exchange content of the functionals yields no clear trends in the cyanide and chloride lattice constants, but the trends in individual bond lengths across the range of compounds closely follow the differences in the ionic radii [43].

(ii) As observed previously in the TMOs [26, 27, 42], the bulk moduli of all compounds increase steadily with Fock exchange content, before falling sharply at the UHF level. Values are in the range from 39 to 53 GPa in the cyanides, and some 1–5 GPa lower in the corresponding chlorides. We attribute the discrepancies in theoretical and experimental [16] values to the differences in the structures studied. The Cr^{III}–C and Cr^{III}–Cl bonds show a similar rate of change of length with pressure in all comparable compounds and Hamiltonians, and are found to be less compressible than the M^{II}–N and M^{II}–Cl bonds. The strong C≡N bonds remain relatively constant in length across the range of pressures accessed.

(iii) The lower ionic charges borne by V^{II} and Cr^{III} ions, and the larger ligand–metal overlap populations indicate a greater degree of covalency in the bonds to these ions as compared with those involving Mn^{II} and Ni^{II} sites. As in the TMOs [26, 27, 42], Hamiltonians containing larger admixtures of Fock exchange yield more ionic ground states. Lattice compression leads to a reduction in the magnitude of the charges at all sites, indicative of a general trend toward a more covalent or metallic ground state, as expected.

(iv) The M^{II} spin moments obtained from Mulliken analyses are all close to the respective spin-only values in the free ions. The presence of large, counter-aligned moments on C and N atoms attests to the presence of strong superexchange interactions in all three PBAs, while the Cl^{-} ions bear only very small moments, as expected. Compression of the lattices leads to reductions in the magnitude of TM spin moments, whereas the C and N moments enlarge progressively across the same range of pressure, both effects arising out of the increase in metal–ligand overlap.

(v) The atom-projected densities-of-states plots for each compound provide direct predictions for the characters of the electron hole and addition states, and for the nature of the fundamental optical excitations. We observe that the band gaps narrow rapidly with increasing pressure.

(vi) The sign and strength of the exchange coupling in each compound is in keeping with the qualitative orbital overlap model discussed in section 1. The $F_0 = 35\%$ Hamiltonian applied in combination with a mean field approach yields critical temperatures for spin ordering in good agreement with experimental values in the $V^{II}Cr^{III}$ and $Ni^{II}Cr^{III}$ PBAs, but leads to underestimated T_C values in the $Mn^{II}Cr^{III}$ system. Bloch's phenomenological relationship (1) provides a reliable description of the variation in the exchange interaction strengths with cell volume in the majority of the compounds studied, save in the $Mn^{II}Cr^{III}$ PBA, where a more complex behaviour emerges.

(vii) The CN^{-} ligand isomerization energies may be readily understood on the basis of a simple model involving the changes in the total crystal field stabilization energies. Calculations incorporating varying concentrations of isomerized ligands reveal that the defect formation energy in the $Mn^{II}Cr^{III}$ system is much higher than in the other lattices, and also indicate a strong tendency for flipped ligands to associate. Isomerization weakens the magnetic coupling in the $V^{II}Cr^{III}$ and $Mn^{II}Cr^{III}$ PBAs, and strengthens it in the $Ni^{II}Cr^{III}$ case.

Acknowledgments

The authors thank Dr William C Mackrodt (University of St Andrews, UK) and Dr Serena Margadonna (University of Edinburgh, UK) for useful and interesting discussions. DSM and CCW acknowledge the support of the UK EPSRC under grant GR/T21615 and the STFC under grant FDPG/033.

References

[1] Ferlay S, Mallah T, Ouahès R, Veillet P and Verdaguer M 1995 *Nature* **378** 701
[2] Egan L, Kamenev K, Papanikolaou D, Takabayashi Y and Margadonna S 2006 *J. Am. Chem. Soc.* **128** 6034
[3] Sato O, Iyoda T, Fujishima A and Hashimoto K 1996 *Science* **272** 704
[4] Zhou P H and Xue D S 2004 *J. Appl. Phys.* **96** 610
[5] Verdaguer M and Girolami G 2004 *Magnetism: Molecules to Materials V* ed J S Miller and M Drillon (Weinheim, DE: Wiley–VCH)
[6] Holmes S M and Girolami G S 1999 *J. Am. Chem. Soc.* **121** 5593
[7] Entley W R and Girolami G S 1994 *Inorg. Chem.* **33** 5165
[8] Papanikolaou D, Kosaka W, Margadonna S, Kagi H, Ohkoshi S and Prassides K 2007 *J. Phys. Chem.* C **111** 8086
[9] Egan L, Kamenev K, Papanikolaou D, Takabayashi Y and Margadonna S 2006 *J. Am. Chem. Soc.* **128** 6034
[10] Kamenev K V, Tancharakorn S, Robertson N and Harrison A 2006 *Rev. Sci. Instrum.* **77** 073905
[11] Bloch D 1966 *Ann. Phys. Fr.* **1** 96
[12] Bloch D, Chaisse F and Pauthene R 1966 *J. Appl. Phys.* **37** 1401
[13] Bloch D 1966 *J. Phys. Chem. Solids* **27** 881
[14] de Jongh L J and Block R 1975 *Physica* B **79** 568
[15] Bloch D and Vettier C 1980 *J. Magn. Magn. Mater.* **15–18** 589
[16] Giriat G, Harrison A, Allan D R, Kamenev K V and Middlemiss D S 2008 *Phys. Rev.* B submitted
[17] Harrison N M, Searle B G and Seddon E A 1997 *Chem. Phys. Lett.* **266** 507
[18] Chan J A, Montanari B, Chan W L and Harrison N M 2005 *Mol. Phys.* **103** 2573
[19] Ruiz E, Rodríguez-Fortea A, Alvarez S and Verdaguer M 2005 *Chem. Eur. J.* **11** 2135
[20] Nishino M, Yoshioka Y and Yamaguchi K 1998 *Chem. Phys. Lett.* **297** 51
[21] Daul C, Rauzy C, Decurtins S, Franz P and Hauser A 2005 *Int. J. Quantum Chem.* **101** 753

[22] Weihe H and Güdel H U 2000 *Comments Inorg. Chem.* **22** 75
[23] Ruiz E, Llunell M and Alemany P 2003 *J. Solid State Chem.* **176** 400
[24] Moreira I de P R, Illas F and Martin R L 2002 *Phys. Rev.* B **65** 155102
[25] Feng X and Harrison N M 2004 *Phys. Rev.* B **70** 092402
[26] Mackrodt W C, Middlemiss D S and Owens T G 2004 *Phys. Rev.* B **69** 115119
[27] Corà F, Alfredsson M, Mallia G, Middlemiss D S, Mackrodt W C, Dovesi R and Orlando R 2004 *Struct. Bond.* **113** 171
[28] Moreira I de P R and Illas F 2006 *Phys. Chem. Chem. Phys.* **8** 1645
[29] Saunders V R, Dovesi R, Roetti C, Orlando R, Zicovich-Wilson C M, Harrison N M, Doll K, Civalleri B, Bush I, D'Arco Ph and Llunell M 2003 *CRYSTAL2003 User's Manual* University of Torino, Torino
[30] Dovesi R, Pisani C and Roetti C 1988 *Hartree–Fock Ab Initio Treatment of Crystalline Systems* (Berlin, DE: Springer)
[31] Pisani C (ed) 1996 *Quantum-Mechanical Ab Initio Calculations of the Properties of Crystalline Materials* (*Springer Lecture Notes in Chemistry* vol 67) (Heidelberg: Springer)
[32] Martin R M 2005 *Electronic Structure: Basic Theory and Practical Methods* (Cambridge: Cambridge University Press)
[33] Becke A D 1988 *Phys. Rev.* A **38** 3098
[34] Vosko S H, Wilk L and Nusair M 1980 *Can. J. Phys.* **58** 1200
[35] Lee C, Yang W and Parr R G 1988 *Phys. Rev.* B **37** 785
[36] Becke A D 1993 *J. Chem. Phys.* **98** 5648
[37] Wiberg K B and Rablen P R 1993 *J. Comput. Chem.* **14** 1504
[38] Born M and Huang K 1998 *Dynamical Theory of Crystal Lattices* (New York: Oxford University Press)
[39] Pascale F, Zicovich-Wilson C M, Lopez F, Civalleri B, Orlando R and Dovesi R 2004 *J. Comput. Chem.* **25** 888
[40] Zicovich-Wilson C M, Pascale F, Roetti C, Saunders V R, Orlando R and Dovesi R 2004 *J. Comput. Chem.* **25** 1873
[41] Zicovich-Wilson C M, Dovesi R and Saunders V R 2001 *J. Chem. Phys.* **115** 9708
[42] Alfredsson M, Price G D, Catlow C R A, Parker S C, Orlando R and Brodholt J P 2004 *Phys. Rev.* B **70** 165111
[43] Shannon R D 1976 *Acta Crystallogr.* A **32** 751
[44] Cox P A 1992 *Transition Metal Oxides, An Introduction to Their Electronic Structure and Properties* (Oxford: Oxford University Press)
[45] Jørgensen C K 1969 *Oxidation Number and Oxidation States* (New York: Springer)
[46] Shriver D F and Atkins P W 1999 *Inorganic Chemistry* 3rd edn (Oxford: Oxford University Press)
[47] Muscat J, Wander A and Harrison N M 2001 *Chem. Phys. Lett.* **342** 397
[48] Néel L 1948 *Ann. Phys. Fr.* **3** 137
[49] Gadet V, Mallah T, Castro I and Verdaguer M 1992 *J. Am. Chem. Soc.* **114** 9213
[50] Greibler W D and Babel D 1982 *Z. Naturf.* b **87** 832
[51] Gadet V 1992 *PhD Thesis* Université Pierre et Marie Curie, Paris